Amino Acids (2011) 40:381–392
DOI 10.1007/s00726-010-0643-y

ORIGINAL ARTICLE

Two coiled-coil regions of *Xanthomonas oryzae* pv. *oryzae* harpin differ in oligomerization and hypersensitive response induction

Zhaolin Ji · Congfeng Song · Xuzhong Lu · Jinsheng Wang

Received: 25 January 2010 / Accepted: 27 May 2010 / Published online: 9 June 2010

Abstract $Hpa1_{Xoo}$ (harpin) is a type III secreted protein of the rice blight bacterial pathogen *Xanthomonas oryzae* pv. *oryzae* that elicits a hypersensitive response (HR) in nonhost tobacco. $Hpa1_{Xoo}$ is predicted to contain two potential coiled-coil (CC) regions, one at the N-terminus with a high probability of formation, and one at the C-terminus with a lower probability of formation. We constructed several CC-equivalent peptides by a chemo-synthetic method, and investigated the structure–function of the predicted $Hpa1_{Xoo}$ CC regions, using biophysical and biochemical approaches. Both peptides elicited an HR in tobacco. Mutant versions of the N- and C-terminal peptides that were predicted to disrupt or favor CC formation were generated. The resulting altered HR activity and oligomerization indicated that the N-terminal CC region is essential for eliciting HR, but the C-terminus is not. The results also indicate that a 14-residue fragment (LDQLLCQLISALLQ) within the N-terminal CC region is a minimal and independent functional element for HR-induction in tobacco leaves. We propose that HR-induction requires a specific oligomerization of the CC regions of $Hpa1_{Xoo}$.

Keywords *Xanthomonas oryzae* · Hpa1 · Coiled-coil · Oligomerization · α-helix · Hypersensitive response

Electronic supplementary material The online version of this article (doi:10.1007/s00726-010-0643-y) contains supplementary material, which is available to authorized users.

Z. Ji · C. Song · J. Wang (✉)
Department of Plant Pathology, Nanjing Agricultural University, Weigang 1, Nanjing 210095, People's Republic of China
e-mail: wangjsh@njau.edu.cn

Z. Ji
e-mail: zhlji@163.com

C. Song
e-mail: songcf@njau.edu.cn

X. Lu
Rice Research Institute, Anhui Academy of Agricultural Sciences, Nongke South Road 40, Hefei 230031, People's Republic of China
e-mail: luxuzhong@yahoo.com.cn

Introduction

Canonical coiled-coils (CCs) consist of two-to-five right-handed amphipathic α-helices that wind around one another to form helical bundles with left-handed supercoils (Lupas 1996a). CC protein sequences are characterized by a heptad repeat of seven amino acids, labeled *a*, *b*, *c*, *d*, *e*, *f*, *g*, where *a* and *d* are preferentially hydrophobic residues (Lupas 1996a; Burkhard et al. 2001). The stability of CCs is mainly achieved by systematic packing of the side chains of the *a* and *d* amino acids into a hydrophobic seam, called "knobs-into-holes" packing, first postulated by Crick (1953). The hydrophobic bonding between *a* and *d* residues at the helical bundle interface provides the driving force for the interaction and influences the CC oligomerization state (Harbury et al. 1993). Electrostatic interactions between charged and polar residues at the *e* and *g* positions in opposing α-helices balance attractive and repulsive forces across the hydrophobic interface, largely defining the specificity and influencing the orientation, oligomerization, and stability of the structure (Zhou et al. 1994; Lupas 1996a; Burkhard et al. 2001; Dutta et al. 2001).

Despite their simplicity, CCs are a common and highly versatile assembly motif, found in a wide range of structural and regulatory proteins with functions ranging from assembly of macromolecular complexes to molecular

recognition (Lupas 1996a; Wolf et al. 1997; Newman et al. 2000; Burkhard et al. 2001). Most known CC proteins are eukaryotic, and CCs have only recently been described as structural elements of prokaryotic proteins. CC domains are found in skeletal proteins, motor proteins, transcription regulators, membrane sensors, and in structural elements that mediate large subunit assemblies, such as in flagella and type IV pili. They are also involved in signal-transduction, molecular recognition, cell stability and movement, and can even form ion channels (Burkhard et al. 2001; Delahay and Frankel 2002).

Many components of the type III secretion systems (TTSS) of enteric pathogens are predicted to share a common CC structural feature (Pallen et al. 1997). Known functions of these secreted proteins include sensing and regulation of secretion, assembly of extracellular structures, and enzyme activity. Evidence from functional studies suggests that CCs are intrinsically involved in subunit assembly, translocation, and in flexible interactions with multiple bacterial and host proteins (Pallen et al. 1997; Delahay and Frankel 2002). None of the 15 effectors secreted by the TTSS of the plant pathogen *Pseudomonas syringae* pv. *tomato* (Guttman et al. 2002) are predicted to have a CC structure; however (Delahay and Frankel 2002). Rairdan et al. (2008) analyzed the role of the CC domain in the potato Rx protein that confers resistance to *Potato virus X*, and found that the highly conserved CC domain five-amino-acid motif, EDVID, mediates an intramolecular interaction that is dependent on the nucleotide-binding and leucine-rich repeat domains of Rx. Other CC domain regions mediate interaction with the Ran GTPase-activating protein, which is required for Rx function. Furthermore, the CC and leucine-rich repeat domains coregulate the signaling activity of the nucleotide-binding domain in a recognition-dependent manner.

Harpins are a class of helper proteins secreted by the TTSS of many Gram-negative phytopathogenic bacteria (Wei et al. 1992; Alfano and Collmer 1997; Kim and Beer 1998). Harpins are encoded by *hrp* (hypersensitive response and pathogenicity) genes that control pathogenicity in susceptible plants and elicit a hypersensitive response (HR) in nonhost plants or resistant host cultivars (Lindgren et al. 1986; Galán and Collmer 1999). The common characteristics of harpins include high glycine content, susceptibility to proteases, high thermal stability, and acidic composition (Wei et al. 1992; Kim and Beer 1998). When harpins infiltrate nonhost plants, they trigger disease resistance-associated defense responses, such as the HR, accumulation of pathogenesis-related gene transcripts, and systemic acquired resistance (Baker et al. 1993; He et al. 1993; Gopalan et al. 1996; Strobel et al. 1996; Dong et al. 1999; Galán and Collmer 1999). HR in plants is an early defense response similar to programmed cell death or apoptosis in animals, and it restricts plant pathogen growth by rapid collapse of challenged tissue (Tarafdar et al. 2009).

The current understanding of the biochemical mechanism of HR induction by harpins in nonhost plants is incomplete, with few studies on this phenomenon. Tarafdar et al. (2009) demonstrated an aggregated state and thermal unfolding in harpin$_{Pss}$ from *Pseudomonas syringae* pv. *syringae*, and used bioinformatics to predict two leucine-zipper-like motifs that may be responsible for aggregation and HR-elicitation. Nonetheless, the detailed mechanism of oligomerization and HR induction are not yet known. The N-terminal α-helix motif of the HpaG harpin, from *X. axonopodis* pv. *glycines*, is critical for fibril formation, which is responsible for HR induction in tobacco (Oh et al. 2007).

Most studies of harpin function and structure have focused on the N-terminal α-helix domain. Although harpin domains have been identified and their sizes compared, few studies have examined the C-terminal α-helix. Alfano et al. (1996) found that HR elicitation by HrpZ (harpin$_{Pss}$) resides in multiple domains, including the N-terminal 109 amino acids and the C-terminal 216 amino acids. However, a molecular understanding of how harpins cause the HR remains unclear. The lack of studies on harpin structure–function relationships motivated us to look for structural motifs in these proteins.

Harpin Hpa1$_{Xoo}$ of *Xanthomonas oryzae* pv. *oryzae* comprises 139 amino acids, with predicted N-terminal and C-terminal α-helical CC structures, that possibly form dimers (Wang et al. 2007). The N-terminal α-helix is implicated in aggregate formation (Wang et al. 2007), and its disruption by the introduction of a proline at residue L51 (L51P) eliminates HR activity in tobacco (Wang et al. 2008).

In this study, we found that Hpa1$_{Xoo}$ self-interacts and forms a complex that contains a monomer and a dimer. We designed and chemosynthesized truncated peptides derived from Hpa1$_{Xoo}$ to investigate the functional and structural role of the CCs. The peptide mutants were compared to wild-type peptides in a wide range of biological and physicochemical tests. We identified a 14-residue independent functional element in the N-terminal CC. Mutant peptides from both CC regions strongly altered HR elicitation and assembly, confirming that the CCs at the N- and C-termini of Hpa1$_{Xoo}$ possess opposing effects on HR elicitation in tobacco leaves. We also used the CC synthetic peptides to investigate harpin structure–function relationships.

Materials and methods

Strains, plasmids, and chemicals

The bacterial strains and plasmids used in this study were derived from Wang et al. (2008). *X. oryzae* pv. *oryzae* was

grown at 28°C in nutrient broth liquid or nutrient broth agar plates. *Escherichia coli* BL21(DE3) was cultivated at 37°C in Luria–Bertani broth liquid (LB) or on LB broth agar plates. Protease inhibitor phenylmethylsulphonyl fluoride (PMSF) was from Shanghai Sangon Biotech Co. Ltd (Shanghai, China), 2,2,2-trifluoroethanol (TFE) was from Alfa Aesar Co. Ltd (Tianjin, China), and inducer isopropyl β-D-thiogalactoside (IPTG) was from EMD Chemicals Inc. (Gibbstown, New Jersey, USA). Protein molecular weight standards for analytical gel filtration were from GE Healthcare Bio-Sciences AB (Uppsala, Sweden). All other chemicals were of analytical grade.

Peptide design and synthesis

Peptides synthesized for this study were designed with following considerations. Peptides were derived from the α-helical domains of the $Hpa1_{Xoo}$ protein. Selected fragments were within the CC-forming region and contained the two heptads of 14 residues. Additional peptides of three heptads (21 amino acid residues) were designed to span the CC-forming region. The hydrophobic residues at position *a* and *d* were presumed to be mainly responsible for the formation and stabilization of the CC. Therefore, these residues were mutated to alter CC formation. Electrostatic attractions between *e* and *g* residues were assumed to partially affect the CC, so these residues were replaced by charged residues to enhance interchain interactions.

Peptides were synthesized by F-moc chemistry and purified by GenScript Corporation (Nanjing, China) and Beijing Genomics Institute HD Biosciences Corporation (Shanghai, China). Purified peptides were characterized by analytical high-performance liquid chromatography (HPLC) and matrix-assisted laser desorption ionization-time of flight mass spectrometry (MALDI-TOF MS). Peptides were stored as solid powders at −20°C.

Circular dichroism (CD) spectroscopy

CD measurements were performed on a Jasco J-810 spectropolarimeter (Jasco Co., Japan) equipped with a Peltier thermoelectric temperature control system and flow-through HPLC cell, controlled by Jasco's Spectra Manager software (Jasco Co., Japan). Wavelength scans were performed at 20°C from 190 to 260 nm at 0.1 nm intervals, at 100 nm/min, with a response time of 1 s per point, and a bandwidth of 1.0 nm in a 0.2-cm-pathlength quartz cell. Peptide concentrations were approximately 40 μM or as indicated in Results, in water or 50% TFE. The far-ultraviolet (UV) CD spectra were the mean of three accumulations with buffer background subtracted. Curves were from triplicate measurements. After baseline correction, ellipticities in mdeg were converted to molar ellipticities (deg cm^2/dmol) by normalizing for peptide bond concentration. Quantitative estimations of secondary structure contents were made using Jasco's Spectra Manager software. For temperature denaturation, thermal unfolding curves were recorded at 222 nm from 20 to 100°C continuously, at a scan rate of 1°C/min.

Size-exclusion chromatography (SEC)

SEC was carried out on a Superdex 30 HiLoad 16/60 PrepGrade column or a Superose 12 10/300 GL column (GE Healthcare Bio-Sciences AB, Sweden) attached to an ÄKTA fast protein liquid chromatography (FPLC) system (Amersham Biosciences AB, Sweden). Peptides and proteins were prepared in 0.5 mL water and injected on a gel-filtration column using running buffer (mobile phase) containing 20 mM Tris–HCl, pH 8.0, and 100 mM KCl. $Hpa1_{Xoo}$ protein and polypeptides were applied to a column equilibrated in running buffer for at least 1 h before injection and eluted with running buffer at a flow rate of 0.8 mL/min at room temperature. The molecular weight of $Hpa1_{Xoo}$ protein from the Superose 12 column was estimated by a calibration program (Amersham Biosciences). A Superdex 30 column was calibrated with peptide standards (3,894, 3,134, 2,365, 1,596, and 827 Da, GE Healthcare Bio-Sciences). Blue dextrin was used to determine the void volume. Molecular masses were determined by plotting log molecular masses of the standards against the partition coefficient (K_{av}), using $K_{av} = (V_e - V_0)/(V_t - V_0)$, where V_e represents elution volume, V_0 is the void volume, and V_t is the total column volume. The calculated protein/peptide complex mass was divided by the bioinformatically determined monomer mass to determine the number of monomers in the complex.

Analytical ultracentrifugation (AUC)

Sedimentation velocity (SV) experiments were performed on a ProteomeLab XL-I analytical ultracentrifuge (Beckman Coulter Inc., USA) equipped with absorbance optics and an An-60 Ti analytical rotor. SV experiments were carried out at 20°C and 60,000 rpm using double-sector aluminum centerpieces with quartz windows. Each sample was scanned at 0-min time intervals for 800 scans. Peptide and protein samples in water or 20 mM Tris–HCl, pH 8.0, 100 mM KCl buffer were run at adaptive concentrations of approximately 0.5 mL, with an equal amount of matched buffer as a reference. Data were analyzed by the continuous distribution [c(s)] method using the SedFit program (http://www.analyticalultracentrifugation.com/default.htm), or by the dc/dt [g(s*)] method using the program DCDT+ (http://www.jphilo.mailway.com/dcdt+.htm). In SV analysis, the shape of the protein concentration profiles correlates

with the homogeneity and diffusion properties of the species in solution, while the rate of movement of the concentration boundary gives the sedimentation coefficient (S).

Hypersensitive response (HR) assays

Tobacco (*Nicotiana tabacum* L. "Xanthi") plants were grown in greenhouses at 25°C, 80% relative humidity, with light for 13 h per day. At 7–8 weeks after planting, leaf panels were infiltrated as previously described (Wei et al. 1992). The needle-less syringe infiltration volume of peptides and proteins was 100 µL. Plants were maintained as described and responses assessed after 24 h. HR photographs were taken 24 h after infiltration. Experiments were repeated at least three times, with six plants infiltrated with each peptide or protein in aqueous solution per experiment.

$Hpa1_{Xoo}$ protein expression and purification

The target DNA *hpa1*$_{Xoo}$ was excised from pMD18-T-*hpa1*$_{Xoo}$ (Wang et al. 2008) by *Nde*I–*Bam*HI digestion and cloned into the *Nde*I–*Bam*HI sites of pET-30a(+). Constructs were transformed into *E. coli* BL21(DE3) and confirmed by sequencing. Saturated overnight cultures of pET-*hpa1*$_{Xoo}$/*E. coli* BL21(DE3) were expanded (1:100) in LB broth (100 mL) supplemented with 30 µg/mL kanamycin and grown at 37°C to OD_{600} of 0.7. Protein expression was induced by 1.0 mM IPTG. Cells were incubated for an additional 4 h at 37°C and collected by centrifugation at 5,000 rpm for 5 min at 4°C. Cell pellets were suspended in 10 mL of ice-cold phosphate buffer (5 mM KH_2PO_4, pH 6.5) and PMSF to 0.5 mM. Aliquots were sonicated five times with 15-s pulses, and 20 s on ice between pulses. Sonicates were centrifuged at 12,000 rpm for 15 min at 4°C. Supernatants were harvested and placed in a boiling water bath for 10 min, centrifuged as described above, and collected as $Hpa1_{Xoo}$ crude supernatants. *E. coli* BL21(DE3) cells with pET-30a(+) were subjected to the same protocol, for pET-30a(+) crude supernatant. All supernatants were stored at −20 or 4°C. The purification of expressed products was by SEC as described above.

Results

Analysis of structure–function of $Hpa1_{Xoo}$ from *E. coli*

SEC was performed to purify $Hpa1_{Xoo}$ and monitor its aggregation states. Crude protein preparations containing *E. coli*-produced $Hpa1_{Xoo}$ showed two peaks (A and B) indicating two components (Fig. 1a). Both fractions A and B induced HR in tobacco leaves (Fig. 1b). Elution volumes were 8.17 mL for fractions A, and 15.11 mL for B. The molecular size for component A was >300 kDa, and component B was approximately 14 kDa.

The CD spectrum of purified fraction A showed two negative peaks with minima at approximately 208 and 222 nm (Fig. 2a). However, the CD spectrum of purified fraction B showed a negative peak with a minimum at 208 nm and a positive peak with a maximum at 265 nm. Quantitative analysis indicated 27.0% α-helix, no β-sheet, 26.2% turn and 46.8% unordered form (random coil) in fraction A, and 17.8% α-helix, 16.6% β-sheet, 23.0% turn, and 42.6% random coil in fraction B.

AUC was conducted to confirm the oligomeric structures of fractions A and B. Fig. 2b and c shows the apparent distributions of S for fractions A and B, with 9.730 for A, and 2.182 for B. Fraction B, however, shows an abnormal peak, while fraction A gave a normal distribution peak. Data fitting gave an apparent molecular mass of 24,440 Da for fraction A and 7,830 Da for fraction B.

Generation of $Hpa1_{Xoo}$ peptides

Secondary structure prediction indicated that $Hpa1_{Xoo}$ (accession number AY205561) harbors two α-helical

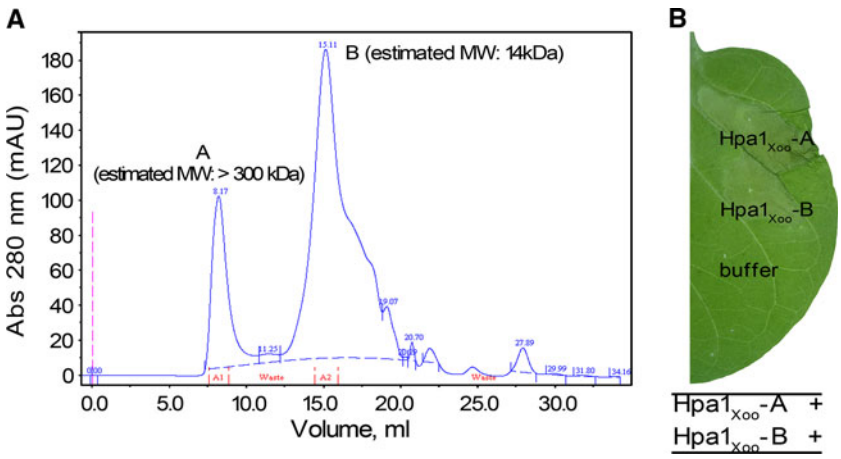

Fig. 1 Purification and HR activity of $Hpa1_{Xoo}$ protein expressed in *E. coli*. **a** SEC elution profiles of expressed $Hpa1_{Xoo}$ using a Superose-12 10/300 GL gel filtration column. The masses of $Hpa1_{Xoo}$ were determined by a calibration program. **b** HR induced in tobacco leaf by elution fractions A and B of $Hpa1_{Xoo}$ crude supernatant. Negative control was 20 mM Tris–HCl, 100 mM KCl

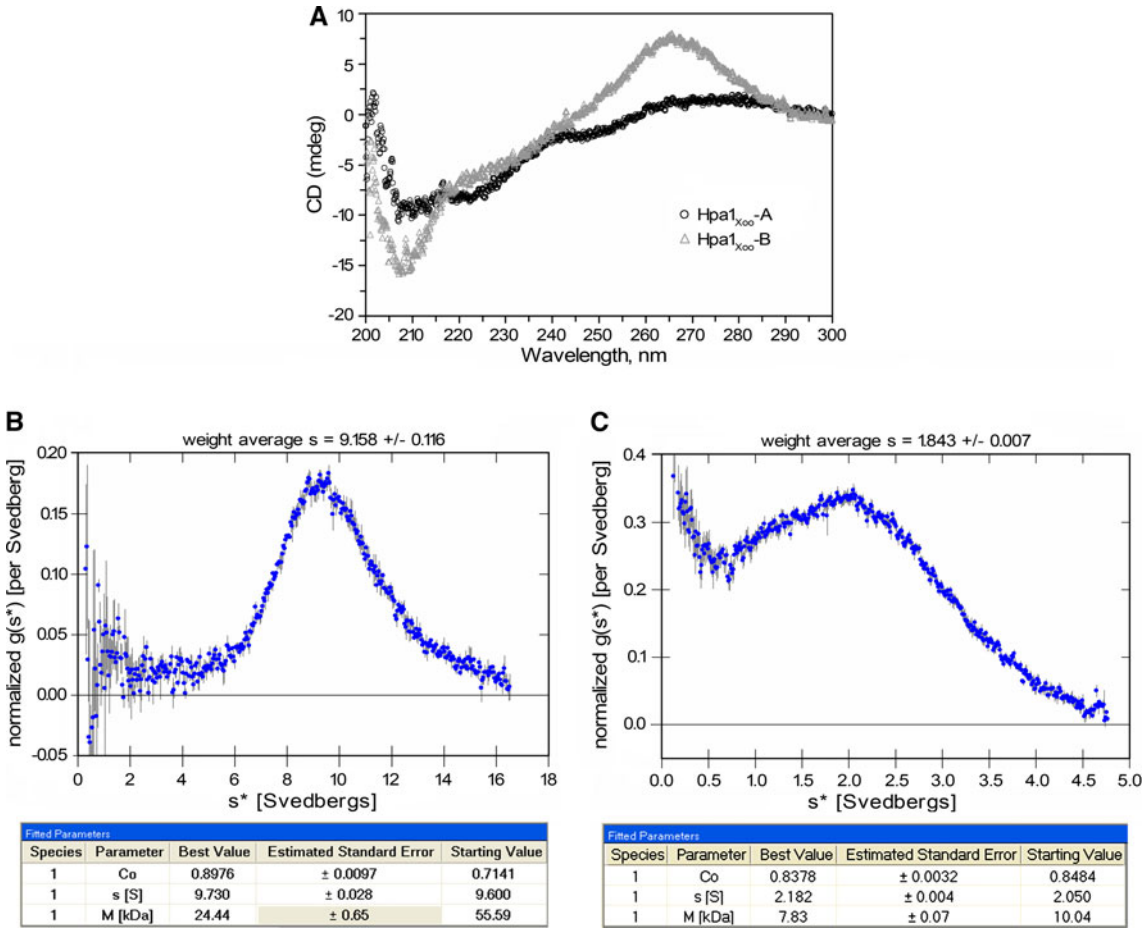

Fitted Parameters

Species	Parameter	Best Value	Estimated Standard Error	Starting Value
1	Co	0.8976	± 0.0097	0.7141
1	s [S]	9.730	± 0.028	9.600
1	M [kDa]	24.44	± 0.65	55.59

Fitted Parameters

Species	Parameter	Best Value	Estimated Standard Error	Starting Value
1	Co	0.8378	± 0.0032	0.8484
1	s [S]	2.182	± 0.004	2.050
1	M [kDa]	7.83	± 0.07	10.04

Fig. 2 Structural analysis of Hpa1$_{Xoo}$ protein expressed in *E. coli*. **a** CD spectra of elution fractions A and B (peaks *A* and *B*, see Fig. 1a) of Hpa1$_{Xoo}$ crude protein. *Black circles* fraction A (*Hpa1$_{Xoo}$-A*); *gray triangles* fraction B (*Hpa1$_{Xoo}$-B*). **b** and **c** AUC analytical profiles and fitted relevant parameters of fractions A and B. AUC data were analyzed by dc/dt [g(s*)] method using the program DCDT+. S, sedimentation coefficient (Svedberg, 1S = 1 × 10^{-13} s); M, molecular weight (kDa); Co, concentration (absorbance value at 280 nm)

regions in the N- and C-termini (Fig. 3a). The COILS program (Lupas et al. 1991; Lupas 1996b) predicted that these α-helical regions had the potential to form CCs, and it also predicted the two CC regions in N- and C-termini. The N-terminal α-helical region had a 0.590 probability of forming a CC in the reference window of 14 residues. However, the C-terminal α-helical domain had only a 0.002 probability. In addition to graphical output, COILS also designates the position of the sequential heptad repeats along the predicted CC sequence, allowing identification of residues in key positions such as *a* and *d* (Fig. 3b).

To investigate the role of the CC regions in Hpa1$_{Xoo}$ function, two peptides and two mutated peptides containing 14 and 21 residues of the N- and C-terminal CC regions were designed and synthesized (Fig. 3b, c). The 14-residue peptide LDQLLCQLISALLQ was named N14 and contained the CC region of N-terminal α-helical domain including the two heptads. The corresponding variant, referred to as N14-L1S, was SDQLLCQLISALLQ, and replaced a hydrophobic leucine residue with a hydrophilic serine at *a* in the first heptad. The 21-residue peptide was PSPFTQMLMHIVGEILQAQNG (C21-1), and the corresponding mutant C21-2, PSPFEQELMHIEGEILQLQNG had four amino acids at *d*, *e*, and *g* changed (Fig. 3c). The CC-forming probability of N14-L1S in Hpa1$_{Xoo}$ decreased to 0.070, and the CC-forming probability of peptide C21-2 increased to 0.708. We also designed a 14-residue peptide WC14 (NQGISEKQLDQLLC), containing two heptads overlapping partially with N14, and containing 12 highly conserved amino acids (H_2N-QGISEKQLDQLL-COOH) (Wang et al. 2007). Peptide purities of the synthetic peptides were all higher than 82%.

Peptide induction of the hypersensitive response

Tobacco leaves infiltrated with aqueous solutions of peptides N14 and C21-1 showed an HR within 24 h (Fig. 4a, b). The

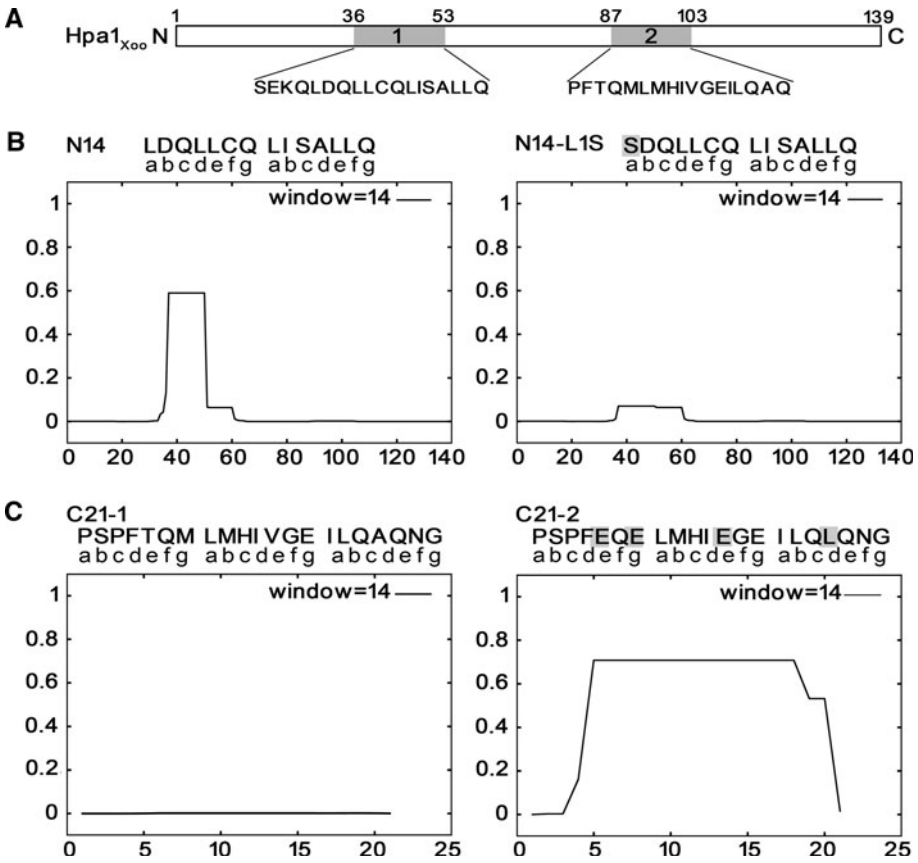

Fig. 3 Schematic representations of $Hpa1_{Xoo}$, amino acid sequences, and CC prediction of $Hpa1_{Xoo}$ truncated peptides. **a** α-helical motifs and corresponding amino acid sequences of $Hpa1_{Xoo}$ protein. The *shaded regions* represent α-helical motifs; the numerical labels indicate the order of the motifs within $Hpa1_{Xoo}$. Motif 1 is a predicted α-helix in the N-terminal region; motif 2 is a predicted α-helix in the C-terminal region. The hierarchical neural network method (HNN, http://npsa-pbil.ibcp.fr/cgi-bin/npsa_automat.pl?page=npsa_nn.html) is used to predict secondary structure. **b** and **c** amino acid sequences and CC-forming probabilities of peptides N14 and N14-L1S, and C21-1 and C21-2 from $Hpa1_{Xoo}$. The CC regions were predicted by the COILS program (http://www.ch.embnet.org/software/COILS_form.html). The letters *a* to *g* designate positions in the heptad repeat. CC forming probability obtained in scanning windows of 14 residues with MTIDK matrix. N14-L1S, L (1) was changed to S in the N14 amino acid sequence. Peptide C21-2 is a four-amino-acid mutant of peptide C21-1 from the C-terminal α-helical region. *Gray boxes* indicate changed amino acids

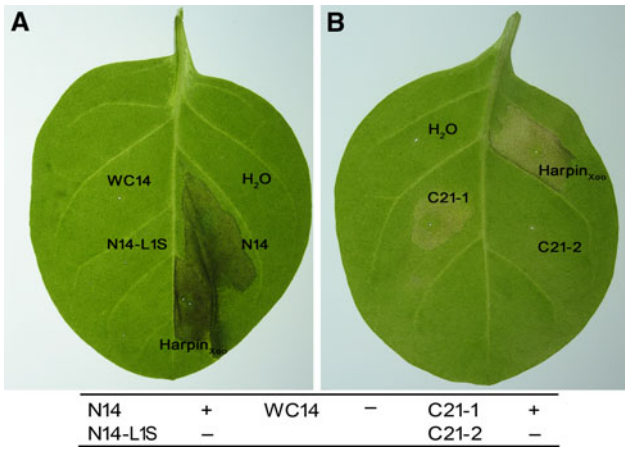

Fig. 4 HR in tobacco induced by synthetic peptides. **a** and **b** truncated $Hpa1_{Xoo}$ peptides N14, N14-L1S, WC14, C21-1 and C21-2. *plus* HR, *minus* no HR

minimum concentration for an HR was 27.8 μM for N14, and 21.3 μM for C21-1 (Supplemental Fig. S1). No HR was seen at concentrations as high as 520.3 μM for WC14, 568.4 μM for N14-L1S, or 412.5 μM for C21-2 (Supplemental Fig. S2).

These data indicated that the N14 peptide, containing 14 amino acids from the N-terminal CC region of $Hpa1_{Xoo}$, was sufficient to cause an HR after infiltrating the intercellular spaces of tobacco leaves. Specifically, the CC domain of the N-terminal α-helix contributed to HR activity, because when the CC-forming possibility was significantly reduced in peptide N14-L1S, no HR was seen in tobacco leaves. The C-terminal α-helical domain appeared to have the opposite effect of the N-terminal domain. When the CC-forming possibility of this peptide was increased, in peptide C21-2, the ability to induce an HR was lost.

Physical and chemical characteristics of the synthesized peptides

CD spectra of N14 presented double minima at 198.5 ± 1 and 225 ± 2 nm, while spectra for N14-L1S presented double minima at 197–202 and 220–225 nm (Supplemental Fig. S3aa). The most distinct difference was the higher ellipticity intensity of the minimum in the short-wavelength region for N14, while N14-L1S exhibited higher intensity in the minimum in the long-wavelength region (Supplemental Fig. S3aa). Since the calculated amount of helix is based on the CD signal at 222 nm ($[\theta]_{222}$), N14 showed no helix, and N14-L1S showed 20.2%. N14 showed no β-sheet, 24.4% turn, and 75.6% random coil. N14-L1S also had no β-sheet, and had 25.7% turn, and 54.1% random coil.

The C-terminal CC region peptide C21-1 in aqueous solution exhibited minima at approximately 208 and 222 nm (Supplemental Fig. S3ba). However, the C21-2 spectrum gave a minimum only at 222 nm. Since the ellipticity at 222 nm of C21-2 was greater than C21-1, the percent α-helix of C21-2 was higher than that of C21-1 (Supplemental Fig. S3ba). C21-1 was 2.3% α-helix, 48.0% β-sheet, 4.2% turn, and 45.5% random coil. C21-2 was 30.1% α-helix, no β-sheet, 25.9% turn, and 44.0% random coil. The CD spectrum of peptide WC14 in aqueous solution presented a minimum at 199 nm (Supplemental Fig. S3ca). This peptide showed no α-helix, 16.7% β-sheet, 20.5% turn, and 62.7% random coil.

Superdex-30 s to analyze the aggregation states of the peptides showed that N14 gave a primary elution peak at 55.44 mL and had a calculated mass size of 3,434 Da (Supplemental Fig. S3ab). Several late peaks were attributed to broken peptide fragments. The mutant N14-L1S gave a different elution profile, mainly presenting as two elution species (Supplemental Fig. S3ac) with estimated molecular weights of 7,775 and 3,940 Da. The double shoulder peaks at 76–80 mL were probably from monomers and partially broken peptide fragments.

C21-1 formed two major elution peaks with elution volumes of 44.61 and 79.58 mL (Supplemental Fig. S3bb), and calculated mass sizes of 6,464 and 920 Da. However, peptide C21-2 exhibited a distinct elution peak at 73.64 mL (Supplemental Fig. S3bc), with a calculated mass size of 1,281 Da. Several late peaks were from broken peptide fragments. The observed masses of 920 and 1,281 Da were smaller than the bioinformatically predicted monomer mass of 2,312 Da for C21-1, and 2,410 Da for C21-2, possibly because the strand helical monomer is difficult to elute from the Superdex-30 column compared to standard spherical proteins.

The WC14 peptide elution profile had three major peaks, with elution volumes of 48.87, 59.75, and 68.99 mL (Supplemental Fig. S3cb), and calculated mass sizes of 5,098, 2,779, and 1,670 Da. The 78.71 mL elution peak probably contained partially broken or degraded monomer polypeptides.

AUC of synthesized peptides was performed only on WC14, and the data fit best to an apparent molecular mass of 3,320 Da (Supplemental Fig. S3cc). Sufficient amounts of the four other peptides, N14, N14-L1S, C21-1, and C21-2 could not be obtained for AUC.

HR-induction and structural characteristics of synthesized $Hpa1_{Xoo}$-N21

We analyzed the CC structure with a 21-residue peptide, NQGISEKQLDQLLCQLISALL, called $Hpa1_{Xoo}$-N21, which contained three heptads, and spanned the α-helical region of the $Hpa1_{Xoo}$ N-terminus. Tobacco leaves infiltrated with an aqueous solution of $Hpa1_{Xoo}$-N21 displayed a strong HR within 24 h (Fig. 5b), and the minimum concentration to elicit an HR was 4.2 μM (Supplemental Fig. S4), which was lower than for N14 and C21-1.

The CD spectrum of $Hpa1_{Xoo}$-N21 had minima at 208 and 222 nm (Supplemental Fig. S5a). $Hpa1_{Xoo}$-N21 was highly α-helical with 59.6% α-helix, 17.8% β-sheet, no turns, and 22.7% random coil. The aggregation state of $Hpa1_{Xoo}$-N21 was determined by AUC and SEC. Data from SV analysis fit best to an apparent molecular weight of 15,468 Da, with little apparent molecular mass at 51,755 Da (Supplemental Fig. S5b). By Superdex-30 gel filtration chromatography analysis, however, the elution profile of $Hpa1_{Xoo}$-N21 presented two peaks of elution volumes 50.72 and 67.92 mL (Supplemental Fig. S5c), and calculated molecular weights of 4,597 and 1,762 Da. The observed mass of 1,762 Da was less than the bioinformatically predicted monomer mass of 2,328 Da, possibly for the same reasons given for the C21 peptides.

HR-induction and structural characteristics of synthesized Hpa1 homologs

To determine whether the fragmental CCs in the N-terminal α-helical domains of Hpa1 homologs in *Xanthomonas* are important for inducing the HR in tobacco, four peptides of 21-residues, each containing three heptads, were synthesized (Fig. 5a).

$Hpa1_{Xoc}$-N21, $Hpa1_{Xoo}$-N21, and $HpaG_{Xag}$-N21 (Hpa_{Xm}-N21 and $Hpa1_{Xac}$-N21) induced a strong HR in tobacco leaves (Fig. 5b), while $Hpa1_{Xcc}$-N21 and $XopA_{Xcv}$-N21 induced no response. The greater potential of the 21-residue peptides to form CCs (Fig. 5c) appeared to confer corresponding HR induction.

In aqueous solution, $Hpa1_{Xoo}$-N21, $Hpa1_{Xoc}$-N21, and $HpaG_{Xag}$-N21 gave similar CD spectra, with double minima

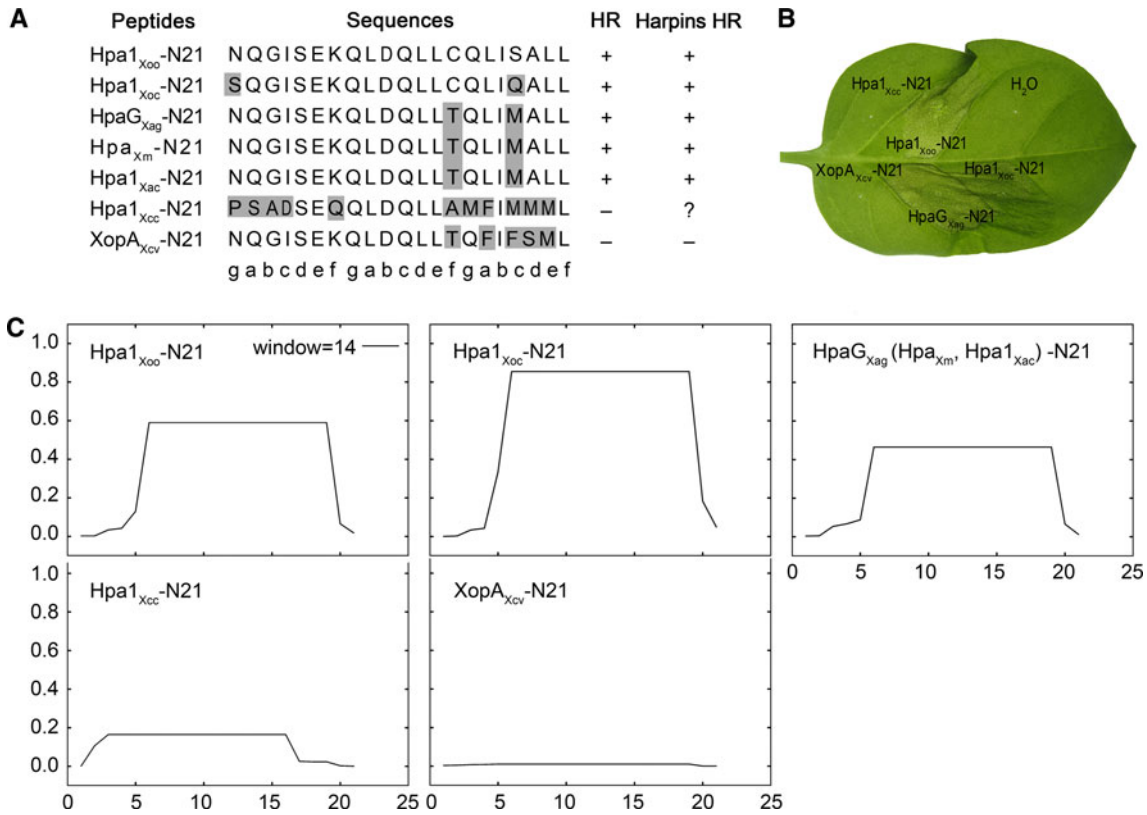

Fig. 5 Sequences, HR-induction, and CC prediction of 21-residue peptides from the N-terminal α-helix of Hpa1 from *Xanthomonas*. **a** and **b** amino acid sequences and HR activities of 21-residue peptides from Hpa1 homologs. Heptad repeat is *a*, *b*, *c*, *d*, *e*, *f*. *g*. The accession numbers in GenBank are $Hpa1_{Xoo}$ (*X. oryzae* pv. *oryzae*) AY205561; $Hpa1_{Xoc}$ (*X. oryzae* pv. *oryzicola*) AY875714; $HpaG_{Xag}$ (*X. axonopodis* pv. *glycines*) AAP34334; Hpa_{Xm} (*X. campestris* pv. *malvacearum*) DQ643828; $Hpa1_{Xac}$ (*X. axonopodis* pv. *citri*) Xac0416; $Hpa1_{Xcc}$ (*X. campestris*. pv. *campestris*) NP_636614; $XopA_{Xcv}$ (*X. campestris* pv. *vesicatoria*) AAL78294. *Gray boxes* indicate amino acids that differ from $Hpa1_{Xoo}$. Peptide purities of $Hpa1_{Xoo}$-N21, $Hpa1_{Xoc}$-N21, $HpaG_{Xag}$-N21, $Hpa1_{Xcc}$-N21 and $XopA_{Xcv}$-N21 are 98.4, 85.9, 78.8, 90.3 and 89.4%, respectively. The amino acid sequence of $HpaG_{Xag}$-N21 was consistent with Hpa_{Xm}-N21, and $Hpa1_{Xac}$-N21. *Plus* HR, *minus* no HR, *question mark* HR not reported. Infiltration concentrations were 21.1 μM for $Hpa1_{Xoo}$-N21, 18.3 μM for $Hpa1_{Xoc}$-N21, 16.6 μM for $HpaG_{Xag}$-N21, 18.7 μM for $Hpa1_{Xcc}$-N21, and 18.2 μM for $XopA_{Xcv}$-N21. **c** CC forming probabilities of 21-residue peptides from Hpa1 homologs

at 208 and 222 nm (Supplemental Fig. S6a). Measured helix structures were 59.6% for $Hpa1_{Xoo}$-N21, 50.6% for $Hpa1_{Xoc}$-N21, and 50.2% for $HpaG_{Xag}$-N21. Aqueous solutions of $Hpa1_{Xcc}$-N21 and $XopA_{Xcv}$-N21, however, were deficient in CD signal. Solutions of the two structures in 50% TFE showed α-helical features, however (data not shown).

We selected $Hpa1_{Xoo}$-N21, $Hpa1_{Xoc}$-N21, and $HpaG_{Xag}$-N21 for variational temperature (VT) CD tests. Thermal denaturation was monitored by CD at 222 nm (Supplemental Fig. S6b, c, d). Thermal melts in aqueous conditions showed the destabilizing effects of higher temperature. Thermal unfolding of $Hpa1_{Xag}$-N21 and $Hpa1_{Xoo}$-N21 showed approximately sigmoidal unfolding curves, as expected for a unique, cooperatively folded structure (Supplemental Fig. S6c, d). The first derivatives of the peptide unfolding curves for $Hpa1_{Xag}$-N21 and $Hpa1_{Xoo}$-N21 were dominated by a single peak, revealing transition midpoints of 41 ± 2 and 68 ± 2°C, respectively (Supplemental Fig. S6c, d). Furthermore, unlike the sigmoidal thermal unfolding curves observed for these peptides, the thermal melting curve of $Hpa1_{Xoc}$-N21 showed less cooperativity, and considerable α-helicity at higher temperatures (Supplemental Fig. S6b).

Discussion

Structures of $Hpa1_{Xoo}$ and synthesized peptides

The CD spectrum of purified fraction A had minima at 208 and 222 nm (Fig. 2a), indicating typical α-helical elements (Chen et al. 1974). However, the positive peak at 265 nm of fraction B may indicate exposed phenylalanine residues. SEC results suggested a polymer and a monomer of $Hpa1_{Xoo}$. The greater fraction B peak area suggested that

expressed $Hpa1_{Xoo}$ protein was predominantly a monomer in solution. Based on a bioinformatically predicted monomer mass of 13.7 kDa for $Hpa1_{Xoo}$, AUC suggested A was a dimer and B was a monomer. The molecular size discrepancy for $Hpa1_{Xoo}$ in the experimental and bioinformatic approaches might be attributed to experimental conditions, error, or self-degradation. Differences in the fraction A size of $Hpa1_{Xoo}$ calculated by AUC and SEC, might be because of protein shape. The SEC size calculation was based on spherical standards (Amersham Biosciences 2002). However, fraction A most likely formed secondary structures, causing earlier SEC elution. As a whole, the results from AUC experiments were consistent with those from SEC. These results indicated that special oligomerization was important in vitro, at least for HR-elicitation function. We suggested that $Hpa1_{Xoo}$ can interact with itself, and form a monomer and dimer complex through the two-stranded α-helical CC structure in the α-helical region.

CD spectra indicated that N14 and N14-L1S displayed atypical α-helix structures, with a hypsochromic shift of approximately 10 nm, compared to the minimum at 208 nm of a standard α-helix (Supplemental Fig. S3aa). Random coil rather than α-helix might be the predominant structural component. The α-helix-inducing solvent TFE is widely used to increase the helicity of single-stranded peptides (Su et al. 1994), so we dissolved peptide N14-L1S in 50% TFE. This solution gave a CD spectrum with typical double minima at 208 and 222 nm, with a higher $[\theta]_{222}$ intensity (Supplemental Fig. S7), indicative of the potential to form a typical α-helix structure. Surprisingly, a 2% TFE solution with N14-L1S acquired the ability to induce HR in tobacco leaves that was similar to N14 (Supplemental Fig. S8). Based on the CD spectra (Supplemental Fig. S3), we suggested that C21-1 was a relatively typical α-helix, and C21-2 was an atypical α-helix structure, and WC14 was a typical random coil. Based on Superdex-30s results (Supplemental Fig. S3), we speculated that N14 was a dimer, and N14-L1S was a multiaggregate mixture of monomers and polymers with approximately five monomers and 2.5 monomers. Peptide C21-1 might mainly form a trimer and a monomer, while C21-2 formed only a monomer. WC14 might be a mixture of trimers, dimers, and monomers by SEC. Based on the peak area, monomer content was found to be greater than the dimer and trimer content. AUC analysis indicated that WC14 was a dimer.

Based on the CD, SV, and SEC results (Supplemental Fig. S5), we suggested that $Hpa1_{Xoo}$-N21 was a typical α-helical secondary structure, and was a mixture of dimers and monomers in aqueous solution. The two elution peaks for $Hpa1_{Xoo}$-N21 were merged into one large peak, probably indicative of monomer–dimer equilibrium. In aqueous solution, $Hpa1_{Xoo}$-N21, $Hpa1_{Xoc}$-N21, and $HpaG_{Xag}$-N21 had a typical α-helical structure; however, $Hpa1_{Xcc}$-N21 and $XopA_{Xcv}$-N21 did not (Supplemental Fig. S6a). VT-CD analysis of $Hpa1_{Xag}$-N21 and $Hpa1_{Xoo}$-N21 indicated that peptide unfolding was a two-state process in which the α-helices were much more stable in the CC conformation (Thompson et al. 1993). $Hpa1_{Xoc}$-N21 gave an approximately linear thermal denaturation curve, indicating that the monomeric α-helices were very stable, which probably contained several overlapping transitions and formed two or more elemental complexes. The VT-CD spectra showed distinct differences between the three peptides (Supplemental Fig. S6), suggesting that they are in different states of aggregation.

Functional heptad domain in the N-terminal CC region of $Hpa1_{Xoo}$

The amino acid sequences of peptides WC14, N14, and N21 of $Hpa1_{Xoo}$ overlap, with the N-terminal 14-residues of N21 corresponding to WC14, and the C-terminal 14 amino acids of N21 corresponding to N14. The possible formation of a two-stranded CC by peptide N21 can be demonstrated schematically, with two identical polypeptide chains of 21 residues interacting in parallel, and in-register (Fig. 6). The second and third heptads of N21 allow hydrophobic interactions at positions a–a' and d–d'. However, hydrophobic interactions in the 1st heptad do not occur. Therefore, we propose that a strong correlation exists between CC stability and HR activity. The CC stability of WC14 was lower than N14, and it showed no HR activity, while N14 did. The fragment of N14 that overlaps the latter two heptads of the N-terminal α-helical motif of $Hpa1_{Xoo}$ is likely to be an independent and critical structure–function domain. Although WC14 has two common heptads with N21, lack of the third heptad of N21 made WC14 incapable of inducing an HR in tobacco leaves. Thus, the third heptad ($Q_gL_aI_bS_cA_dL_eL_f$) is a necessary element for eliciting the HR.

Different roles of $Hpa1_{Xoo}$ N- and C-terminal CC formation and implication on oligomerization in HR induction

Our data showed that the CC region plays a critical role in the structure and function of the *Xanthomonas* hpa1 protein. Wild type peptide N14 with higher possibility of forming a CC predicted by COILS program had the ability to induce HR in tobacco leaves, while its mutational peptide N14-L1S with little possibility of CC information eliminated HR activity in tobacco leaves. This indicated that CC formation in N-terminal $Hpa1_{Xoo}$ may be in relation to HR induction. This effect could be due to conformational changes caused by the mutations, affecting the

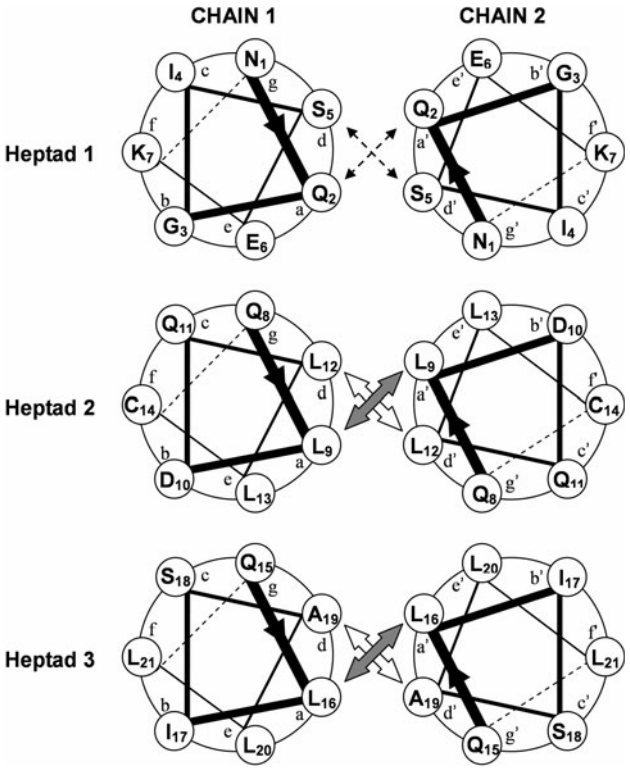

Fig. 6 Schematic of two-stranded, α-helical coiled coils by dimerization of peptide $Hpa1_{Xoo}$-N21. Chains are in register and parallel. *a–g* and *a′–g′* designate positions in the heptad repeat. *Number* following the capital letter indicates amino acid position in the peptide from the N-terminus. Hydrophobic residues at *a–a′* and *d–d′* interact and are responsible for formation and stabilization of the coiled coil. Hydrophobic interactions that do not occur in heptad 1 are indicated by dashed arrows. Electrostatic attractions of intrachain interactions and interchain interactions (*g–e′* or *g′–e*) do not occur

CC domains that might mediate assembly. These structural changes were confirmed by CD and SEC (Supplemental Fig. S3). CD spectra studies revealed that the conformations of mutant peptides were distinctly altered in both secondary structure and content. By SEC, we found that N14 formed a dimer in aqueous solution, and that N14-L1S existed as multiple aggregates of 5, 2.5, and individual monomers. In addition, wild-type peptide $Hpa1_{Xoo}$-N21 with higher possibility of forming a CC had HR-inducting activity in tobacco leaves and presented typical α-helical structure by CD analysis and had dimer form by SEC analysis. The dimers of N14 and $Hpa1_{Xoo}$-N21 were consistent with a two-stranded α-helical CC structure and may be formed by CC structure. We suggest that the interchain a–a′ and d–d′ hydrophobic interactions provide the driving force for the CC formation and influences CC oligomerization state (Fig. 6). Thus, we propose that the dimers from N-terminus of $Hpa1_{Xoo}$ possessed HR-inducing function.

In the C-terminal α-helical domain of $Hpa1_{Xoo}$, however, the contrary is true. Wild type peptide C21-1 has little probability of forming a CC structure and induces an HR in tobacco leaves, while mutational peptide C21-2 with higher possibility of forming a CC led to failure to induce an HR. By CD, we found that C21-1 had a relatively typical α-helix secondary structure, while C21-2 did not. C21-1 with typical α-helix has the potential to form CC structure. By SEC, C21-1 was present as monomers and trimers, and C21-2 was exclusively a monomer in aqueous solution. Accordingly, we propose that the C21 trimer oligomerization form is required for HR induction in tobacco and may be formed by three-stranded α-helical CC structure, while the monomeric form is not. In summary, CC regions at the N- and C-termini of $Hpa1_{Xoo}$ have reverse effects on HR induction in tobacco, with the CC region indispensable for the HR in the $Hpa1_{Xoo}$ N-terminus, but not involved at the $Hpa1_{Xoo}$ C-terminus.

Based on previous mutations in the N-terminal coding region of $Hpa1_{Xoo}$ and $Hpa1_{Xoc}$, we proposed that the function of the C-terminal α-helical domain was suppression in full-length harpin, since N-terminal mutations containing an integrated C-terminal region could not induce an HR in tobacco (Wang et al. 2008). In addition, the C-terminal region of $HrpZ_{Pss}$ (Alfano et al. 1996) and $HrpZ_{Pph}$ (Lee et al. 2001) is sufficient and necessary for HR induction. However, in HrpN from *Erwinia amylovora*, the C-terminal half is not required for cell-free elicitor activity, while the N-terminal half mediates cell-free elicitor activity (Sinn et al. 2008).

A two-heptad CC is the shortest independent element for HR-elicitation in tobacco

We found that the peptide N14 from the N-terminal CC region of $Hpa1_{Xoo}$ induced an HR in tobacco leaves. So far, it is the smallest independent functional element from harpin proteins that possesses HR-inducing ability in the nonhost tobacco. However, the CD spectrum of N14 in aqueous solution shows features typical of both turns and random coils (Supplemental Fig. S3aa). Su and co-workers (Su et al. 1994) demonstrated that CD spectral features and molar ellipticities were significantly affected by the chain length of a peptide designed as a two-stranded α-helical CC. Peptides of less than 19 residues did not have CD spectra of typical α-helical proteins, but contained turns and random coils, consistent with our CD spectra for N14. A likely explanation is the difficulty of CD signal detection for shortchain peptides. Superdex-30s analysis showed that peptide N14 in aqueous solution distinctly existed as a dimer, consistent with a two-stranded α-helical CC structure.

For the minimum number of contiguous heptad repeats required to achieve a stably folded CC, three or four heptad repeats appear to be sufficient for stable CC folding (Lumb et al. 1994; Su et al. 1994). Burkhard et al. (2000; 2002)

and Meier et al. (2002) described the design and characterization of a two-heptad CC system with 15 amino acids, which was stabilized by hydrophobic interactions and a network of salt bridge interactions. However, at increased ionic strength, the dimer state switched to trimer, indicative of poor oligomer-state specificity. These data suggested that N14 possibly formed a two-heptad CC system that was stabilized by hydrophobic interactions and retained HR-inducing ability. In addition, this result also indicated that the sequence of N14 is the primary determinant for $Hpa1_{Xoo}$ function.

This paper focused on the α-helical CC regions as independent structures of $Hpa1_{Xoo}$, and may provide clues to the mechanisms by which harpin-related proteins induce an HR. In combination with amino acid substitutions in vitro, it provides more information on the structure–function relationships in this group of proteins. Our results suggest that the CC region of $Hpa1_{Xoo}$ plays an important role in inducing an HR in tobacco plants. However, the C-terminal CC domain has a negative effect on this process. The 14-residue peptide N14 is the minimal independent unit which can induce an HR. Screening for isolation and identification of receptors (Cooper 2004) will be helpful for a full understanding of the $Hpa1_{Xoo}$ structure and its interaction with plants.

Acknowledgments This work was supported by grants from the National Key Basic Research Plan of China (2003CB114204 and 2006CB101902), the National Key project of China (2004BA901A36), and the Key Project of Science and Technology of Jiangsu (BE-2005-604).

References

Alfano JR, Collmer A (1997) The type III secretion pathway of plant pathogenic bacteria: trafficking harpins, Avr proteins and death. J Bacterial 179:5655–5662

Alfano JR, Bauer DW, Milos TM, Collmer A (1996) Analysis of the role of the *Pseudomonas syringae* pv. *syringae* HrpZ harpin in elicitation of the hypersensitive response in tobacco using functionally non-polar *hrpZ* deletion mutations, truncated HrpZ fragments, and *hrmA* mutations. Mol Microbiol 19:715–728

Amersham Biosciences (2002) Gel filtration: principles and methods. GE Healthcare Bio-Sciences AB, Björkgatan 30, 751 84 Uppsala, Sweden

Baker CJ, Orlandi EW, Mock NM (1993) Harpin, an elicitor of the hypersensitive response in tobacco caused by *Erwinia amylovora*, elicits active oxygen production in suspension cells. Plant Physiol 102:1341–1344

Burkhard P, Meier M, Lustig A (2000) Design of a minimal protein oligomerization domain by a structural approach. Prot Sci 9:2294–2301

Burkhard P, Stetefeld J, Strelkov SV (2001) Coiled coils: a highly versatile protein folding motif. Trends Cell Biol 11:82–88

Burkhard P, Ivaninskii S, Lustig A (2002) Improving coiled-coil stability by optimizing ionic interactions. J Mol Biol 318:901–910

Chen YH, Yang JT, Chau KH (1974) Determination of the helix and beta form of proteins in aqueous solution by circular dichroism. Biochemistry 13:3350–3359

Cooper MA (2004) Advance in membrane receptor screening and analysis. J Mol Recognit 17:286–315

Crick FC (1953) The packing of α-helices: simple coiled coils. Acta Crystallogr A 6:689–697

Delahay RM, Frankel G (2002) Coiled-coil proteins associated with type III secretion systems: a versatile domain revisited. Mol Microbiol 45:905–916

Dong H, Delaney TP, Beer SV (1999) Harpin induces disease resistance in *Arabidopsis* through the systemic acquired resistance pathway mediated by salicylic acid and the *NIM1* gene. Plant J 20:207–215

Dutta K, Alexandrov A, Huang H, Pascal SM (2001) pH-induced folding of an apoptotic coiled-coil. Protein Sci 10:2531–2540

Galán JE, Collmer A (1999) Type III secretion machines: bacterial devices for protein delivery into host cells. Science 284:1322–1328

Gopalan S, Wei W, He SY (1996) *hrp* gene-dependent induction of *hin1*: a plant gene activated rapidly by both harpins and the avr*Pto* gene-mediated signal. Plant J 10:591–600

Guttman DS, Vinatzer BA, Sarkar SF, Ranall MV, Kettler G, Greenberg JT (2002) A functional screen for the type III (Hrp) secretome of the plant pathogen *Pseudomonas syringae*. Science 295:1722–1726

Harbury PB, Zhang T, Kim PS, Alber T (1993) A switch between two-, three-, and four-stranded coiled-coils in GCN4 leucine zipper mutants. Science 262:1401–1407

He SY, Huang HC, Collmer A (1993) *Pseudomonas syringae* pv. *syringae* $harpin_{Pss}$: a protein that is secreted via the hrp pathway and elicits the hypersensitive response in plants. Cell 73:1255–1266

Kim JF, Beer SV (1998) HrpW of *Erwinia amylovora*, a new harpin that contains a domain homologous to pectate lyases of a distinct class. J Bacteriol 180:5203–5210

Lee J, Klessig DF, Nurnberger T (2001) A harpin binding site in tobacco plasma membranes mediated activation of the pathogenesis-related gene *HIN1* independent of extracellular calcium but dependent on mitogen-activated protein kinase activity. Plant Cell 13:1079–1093

Lindgren PB, Peet RC, Panopoulos NJ (1986) Gene cluster of *Pseudomonas syringae* pv. "*phaseolicola*" controls pathogenicity of bean plants and hypersensitivity on nonhost plants. J Bacteriol 168:512–522

Lumb KJ, Carr CM, Kim PS (1994) Subdomain folding of the coiled-coil leucine-zipper from the bZIP transcriptional activator GCN4. Biochemistry 33:7361–7367

Lupas AN (1996a) Coiled coils: new structures and new functions. Trends Biochem Sci 21:375–382

Lupas AN (1996b) Prediction and analysis of coiled-coil structures. Methods Enzymol 266:513–525

Lupas AN, Van Dyke M, Stock J (1991) Predicting coiled coils from protein sequences. Science 252:1162–1164

Meier M, Lustig A, Aebi U, Burkhard P (2002) Removing an interhelical salt bridge abolishes coiled-coil formation in a de novo designed peptide. J Struct Biol 137:65–72

Newman JR, Wolf E, Kim P (2000) A computationally directed screen identifying interacting coiled coils from *Saccharomyces cerevisiae*. Proc Natl Acad Sci U S A 97:13203–13208

Oh J, Kim JG, Jeon E, Yoo CH, Moon JS, Rhee S, Hwang I (2007) Amyloidogenesis of type III-dependent harpins from plant pathogenic bacteria. J Biol Chem 282:13601–13609

Pallen MJ, Dougan G, Frankel G (1997) Coiled-coil domains in proteins secreted by type III secretion systems. Mol Microbiol 25:423–425

Rairdan GJ, Collier SM, Sacco MA, Thomas T, Baldwin TT, Boettrich T, Moffetta P (2008) The coiled-coil and nucleotide binding domains of the potato Rx disease resistance protein function in pathogen recognition and signaling. Plant Cell 20:739–751

Sinn JP, Oh CS, Jensen PJ, Carpenter SC, Beer SV, McNellis TW (2008) The C-terminal half of the HrpN virulence protein of the fire blight pathogen *Erwinia amylovora* is essential for its secretion and for its virulence and avirulence activities. Mol Plant Microbe Interact 21:1387–1397

Strobel RN, Gopalan JS, Kuc JA, He SY (1996) Induction of systemic acquired resistance in cucumber by *Pseudomonas syringae* pv. *syringae* 61 $HrpZ_{pss}$ protein. Plant J 9:431–439

Su JY, Hodges RS, Kay CM (1994) Effect of chain length on the formation and stability of synthetic alpha-helical coiled coils. Biochemistry 33:15501–15510

Tarafdar RK, Vedantam LV, Kondreddy A, Podile AR, Swamy MJ (2009) Biophysical investigations on the aggregation and thermal unfolding of $harpin_{Pss}$ and identification of leucine-zipper-like motifs in harpins. Biochim Biophys Acta 1794:1684–1692

Thompson KS, Vinson CR, Freire E (1993) Thermodynamic characterization of the structural stability of the coiled-coil region of the bZIP transcription factor GCN4. Biochemistry 32:5491–5496

Wang XY, Li M, Zhang JH, Zhang Y, Zhang GY, Wang JS (2007) Identification of a key functional region in harpins from *Xanthomonas* that suppresses protein aggregation and mediates harpin expression in *E. coli*. Mol Biol Rep 34:189–198

Wang XY, Song CF, Miao WG, Ji ZL, Wang XB, Zhang Y, Zhang JH, Hu JS, Borth W, Wang JS (2008) Mutations in the N-terminal coding region of the harpin protein Hpa1 from *Xanthomonas oryzae* cause loss of hypersensitive reaction induction in tobacco. Appl Microbiol Biotechnol 81:359–369

Wei ZM, Laby RJ, Zumoff CH, Bauer DW, He SY, Collmer A, Beer SV (1992) Harpin, elicitor of the hypersensitive response produced by the plant pathogen *Erwinia amylovora*. Science 257:85–88

Wolf E, Kim PS, Berger B (1997) MultiCoil: a program for predicting two- and three-stranded coiled coils. Protein Sci 6:1179–1189

Zhou NE, Kay CM, Hodges RS (1994) The role of interhelical ionic interactions in controlling protein folding and stability. De novo designed synthetic two-stranded α-helical coiled-coils. J Mol Biol 237:500–512